Coating iron oxide nanoparticles with mesoporous silica reduces their interaction and impact on *S. oneidensis* MR-1

Joseph T. Buchman, Thomas Pho, Rebeca S. Rodriguez, Z. Vivian Feng, Christy L. Haynes

PII: S0045-6535(19)31735-7

DOI: https://doi.org/10.1016/j.chemosphere.2019.124511

Reference: CHEM 124511

To appear in: *ECSN*

Received Date: 29 May 2019

Revised Date: 1 August 2019

Accepted Date: 2 August 2019

Please cite this article as: Buchman, J.T., Pho, T., Rodriguez, R.S., Feng, Z.V., Haynes, C.L., Coating iron oxide nanoparticles with mesoporous silica reduces their interaction and impact on *S. oneidensis* MR-1, *Chemosphere* (2019), doi: https://doi.org/10.1016/j.chemosphere.2019.124511.

Coating Iron Oxide Nanoparticles with Mesoporous Silica Reduces their Interaction and Impact on *S. oneidensis* MR-1

Joseph T. Buchman[§], Thomas Pho[‡], Rebeca S. Rodriguez[§], Z. Vivian Feng[‡], Christy L. Haynes*[§]

[§]Department of Chemistry, University of Minnesota, 207 Pleasant St SE, Minneapolis, Minnesota 55455, United States

[‡]Chemistry Department, Augsburg University, 2211 Riverside Ave, Minneapolis, Minnesota 55454, United States

Abstract

Here, we investigate the impact of iron oxide nanoparticles (IONPs) and mesoporous silica-coated iron oxide nanoparticles (msIONPs) on *S. oneidensis* in an aerobic environment, which is likely the main environment where such nanoparticles will end up after use in consumer products or biomedical applications. Monitoring the viability of *S. oneidensis*, a model environmental organism, after exposure to the nanoparticles reveals that IONPs promote bacterial survival, while msIONPs do not impact survival. These apparent impacts are correlated with association of the nanoparticles with the bacterial membrane, as revealed via TEM and ICP-MS studies, and upregulation of membrane-associated genes. However, similar survival in bacteria was observed when exposed to equivalent concentrations of released ions from each nanomaterial, indicating that aqueous nanoparticle transformations are responsible for the observed changes in bacterial viability. Therefore, this work demonstrates that a simple mesoporous silica coating can control the dissolution of the IONP core by greatly reducing the amount of released iron ions, making msIONPs a more sustainable option to reduce perturbations to the environment upon release of nanoparticles into the environment.

Keywords

Nanotoxicity, bacteria, iron oxide, silica, dissolution, gene expression

1. Introduction

The applications of magnetic iron oxide nanoparticles can range from data storage[1] to biomedical imaging and various therapies.[2,3] With such widespread use of these inexpensive and easy-to-synthesize nanomaterials, it is inevitable that some of the nanomaterials will end up in environment. Therefore, it is critical to understand the potential environmental impact of these nanomaterials after their release, especially into aquatic environments.

Given that iron oxide nanoparticles (IONPs) are often susceptible to aggregation when in suspension with complex biological milieu, a silica shell is commonly added to the iron oxide nanoparticle core to improve their stability in complex matrices,[4,5] expanding the range of their

utility for different applications. Since a mesoporous silica coating has pores in its structure, this method of capping nanoparticles still allows access by water to the core material, an attribute that is critical for performance in a variety of biomedical applications.[6] For example, literature has shown, when using iron oxide nanoparticles to image tumors in mice, that use of the mesoporous silica shell is required to stabilize the iron oxide nanoparticles so their magnetic properties facilitate the acquisition of images.[7] With the relevance of this particular platform (mesoporous silica-coated iron oxide nanoparticles) in mind, as well as the general concept of pursuing nanoparticle design motifs that control a nanoparticle's effect on our ecosystem, this work explores the impact of iron oxide and mesoporous silica-coated iron oxide nanoparticles on a model bacterium, *Shewanella oneidensis* MR-1.

Bacteria are used as a surrogate for environmental health due to their important role as decomposers to recycle nutrients for use by other organisms. Therefore, any impacts on bacteria due to nanoparticle interaction could also ultimately affect other environmental organisms. *S. oneidensis* MR-1, specifically, is commonly considered for bioremediation since it is capable of respiring many different metals and is therefore an important part of the geochemical nutrient cycle.[8] *S. oneidensis* has three main mechanisms through which it respires metals (like the constituents of the iron oxide nanoparticles under consideration here): direct interactions with cytochromes on the bacterial surface, the secretion of flavins for extracellular reduction, and growth of electrically conductive pili capable of metal reduction. *S. oneidensis* synthesizes many different cytochromes, including cytochrome *c*,[9] and these cytochromes can be found associated with the outer membrane, periplasmic space, and inner membrane. The system of cytochromes is capable of reducing metals when they come into direct contact with the outer membrane-associated cytochromes.[10,11] *S. oneidensis* also secretes flavins, which are capable of extracellular electron transfer at distances greater than 50 μm from the bacterial cell surface.[12] The flavin system is intimately linked with the outer membrane-associated cytochromes since they shuttle electrons from the cytochromes to the

63 extracellular metals.[13] The third mechanism for *S. oneidensis* to reduce extracellular metals is
64 through direct contact with nanowires, which can grow to be longer than 10 μm.[14] However, it
65 has been demonstrated that the nanowires are only present in significant quantities on *S.*
66 *oneidensis* when grown under O_2-limited conditions,[14] and therefore are not relevant in the
67 conditions considered herein.

68 Iron oxides are among the materials that *S. oneidensis* is capable of reducing.[9,15,16] Often,
69 under anaerobic conditions, *S. oneidensis* reduces iron oxides to synthesize extracellular
70 magnetite.[17–19] For example, when direct contact is made with hematite NPs, *S. oneidensis*
71 reduces them to form magnetite nanoparticles.[20,21] *S. oneidensis* has also demonstrated an
72 ability to dissolve and reduce magnetite.[22,23] While many of these studies are performed
73 anaerobically, a related species of *S. oneidensis, S. putrefaciens* 200R, has been shown to
74 attach to magnetite at similar levels under both aerobic and anaerobic conditions.[24] It has also
75 been observed that some reduction machinery is upregulated in *S. oneidensis* MR-1 under
76 aerobic conditions.[25] Furthermore, there is evidence that nitrate can be respired in aerobic
77 conditions, as well as nitrite and fumarate, which can also be respired, but only after bacteria
78 have entered the stationary phase; this is true for several electron acceptors that have been
79 studied.[26,27] While there are many studies exploring the relationships between *S. oneidensis* and
80 bulk iron oxides, there is a dearth of literature looking at the interactions of nanoscale magnetite
81 with *S. oneidensis*. Given that nanoparticles have a much higher surface area to volume ratio
82 than their bulk counterparts, which imparts unique physicochemical properties to particles at the
83 nanoscale, simply extrapolating the interactions of *S. oneidensis* with bulk iron oxide to
84 nanoscale iron oxide may not wholly account for these increased complexities.

85 Herein, we report the interactions between *S. oneidensis* and iron oxide nanoparticles, and
86 then detail our use of a mesoporous silica coating around the IONPs to mitigate their impact.
87 The studies presented here investigate the impact of nanoscale magnetite under aerobic
88 conditions, as those are likely to be the prevailing conditions in aquatic environments where

nanoparticles are released. Colony counting was utilized to investigate the impact on bacterial survival after nanoparticle exposure. To understand the differential survival, the binding of the nanoparticles was investigated with TEM and ICP-MS. The contribution of ion release by the nanoparticles was assessed, and any impact on the production of riboflavin was investigated with HPLC. To probe these differences even further, changes in gene expression in *S. oneidensis* was analyzed using quantitative reverse transcription polymerase chain reaction (RT-qPCR). These studies showed that IONPs promote bacterial survival through the release of iron ions, and that, by reducing ion dissolution, the addition of a mesoporous silica coating mitigates that impact.

2. Experimental

2.1 Materials

Chloro-trimethyl silane was obtained from Fluka and 2-[methoxy(polyethyleneoxy)$_{9\text{-}12}$propyl]-trimethoxysilane, tech 90 (PEG-silane, molecular weight 591-723 g/mol, 9-12 EO) was purchased from Gelest, Inc. (Morrisville, PA). EMG 308 Ferrofluid was acquired from Ferrotec (Santa Clara, CA). RNAzol® RT was acquired from Molecular Research Center, Inc. (Cincinnati, OH) and iTaq™ Universal SYBR® Green Supermix was obtained from Bio-Rad Laboratories, Inc. (Hercules, CA). Deoxyribonucleotides, random primers, SuperScript III reverse transcriptase, and RNaseOUT™ recombinant ribonuclease inhibitors were acquired from Invitrogen (Carlsbad, CA). Primers for specific genes for *S. oneidensis* were purchased from Integrated DNA Technologies (Skokie, IL). *Shewanella oneidensis* MR-1 was graciously provided by Dr. Jeffrey Gralnick (Dept of Microbiology, University of Minnesota). All other materials used are listed in the Supplementary Information.

2.2 Synthesis of Mesoporous Silica and Mesoporous Silica-coated Iron Oxide Nanoparticles

To synthesize MSNs, a previously published protocol was adapted and used.[28] Briefly, cetyltrimethylammonium bromide (0.29 g) was mixed with 150 mL of 0.36 M NH_4OH [*caution:*

concentrated NH_4OH is both toxic and corrosive!] and stirred (1 h, 300 rpm, 50 ℃). Then, 2.5 mL of 0.88 M tetraethylorthosilicate in ethanol was added dropwise and stirred (1 h, 600 rpm, 50 ℃), followed by slow addition of 450 µL of 2-[methoxy(polyethyleneoxy)9-12propyl]-trimethoxysilane and stirring (30 min, 600 rpm, 50 ℃). Finally, 68 µL of chlorotrimethylsilane were added and stirred (30 min, 600 rpm, 50 ℃) with the beaker covered.

A previously published method was used to prepare msIONPs.[7] Since the purchased IONPs have an anionic, proprietary ligand on their surface, they were first overcoated with PVP-10, a hydrophobic coating that will allow for favorable interactions with the hydrophobic tails of CTAB, used later in the synthesis. To make the EMG 308/surfactant suspension, the following materials were added sequentially into 5 mL of ultrapure water while sonicating, with 1 h sonication steps between each addition: 0.6 g PVP-10, 400 µL EMG 308 suspension, and 0.29 g CTAB. To an Erlenmeyer flask, 145 mL of ultrapure water was added. While sonicating, the EMG 308/surfactant suspension was added dropwise; sonication continued for another hour to ensure dispersity. The temperature was increased to 50 ℃, and the suspension was stirred (15 min, 300 rpm). Then, 2.5 mL of 28% NH_4OH was added and stirred (15 min, 300 rpm, 50 ℃), followed by dropwise addition of 2.5 mL of 0.88 M ethanolic tetraethylorthosilicate with stirring (1 h, 700 rpm, 50 ℃). Slowly, 450 µL of 2-[methoxy(polyethyleneoxy)$_{9-12}$propyl]-trimethoxysilane was added and then stirred (30 min, 700 rpm, 50 ℃) and lastly, 68 µL of chlorotrimethylsilane was added and stirred (30 min, 700 rpm, 50 ℃) with the flask covered by a glass Petri dish. The suspension was then transferred to a clean 250 mL Erlenmeyer flask without a stir bar.

For gentle evaporation, both MSNs and msIONPs were then aged at 50 ℃ for ~20 h (care was taken so that not all solvent evaporated), followed by hydrothermal treatment at 90 ℃ for 24 h to improve particle stability. Oxygen was removed from msIONPs prior to hydrothermal treatment by purging the reaction vessel and suspension with nitrogen gas to reduce oxidation of the cores at the higher temperatures of hydrothermal treatment. The NPs were purified by ultracentrifugation (30 min, 61,579×*g*) and resuspension in 50 mL 6 g/L NH_4NO_3 for reflux (1 h,

300 rpm, 60 ℃). The suspension was then ultracentr ifuged (all subsequent ultracentrifugation steps were done for 20 min at 61,579×*g*) and resuspended in 95% ethanol. This was ultracentrifuged and resuspended in 6 g/L NH_4NO_3 to reflux again (1 h, 300 rpm, 60 ℃). The suspension was ultracentrifuged three more times and resuspended in the following order: 95% ethanol, 99% ethanol, 99% ethanol. The final suspension was filtered through a 0.2 μm GHP syringe filter.

2.3 Transmission Electron Microscopy

To prepare the nanoparticles for imaging by transmission electron microscopy, they were first diluted to a suspension of approximately 0.5 mg/mL (IONPs were used at ~2 mg/mL) and sonicated for 10 min to ensure dispersal. Then, for MSNs and msIONPs, a 200 mesh copper grid with Formvar and carbon supports (Ted Pella, Inc., Redding, CA) was briefly dipped into the suspension. For IONPs, a 3 μL drop of the suspension was placed onto the grid surface. All grids were dried near an open 65 °C oven prior to imaging with a FEI Tecnai T12 transmission electron microscope. To acquire the images, the microscope was used at an operating voltage of 120 kV. Size analysis was performed on the images using ImageJ,[29] with size determined by measuring the diameter of at least 500 randomly chosen nanoparticles (it is assumed that all nanoparticles are spherical) using built-in functions of ImageJ.

2.4 Hydrodynamic Diameter and Zeta Potential Measurements

To determine the hydrodynamic diameter and zeta potential of the nanoparticles used in this study, the nanoparticles were first suspended in water at a concentration of 0.5 mg/mL. The hydrodynamic diameters and ζ-potentials were then analyzed using a Brookhaven ZetaPALS instrument. The stability of the nanoparticles in the exposure medium (HEPES buffer) was also assessed by suspending the nanoparticles (300 μg/mL) in HEPES buffer and checking their hydrodynamic diameter after 30, 60, and 120 min.

2.5 Bacterial Culture Conditions

S. oneidensis MR-1 was stored at -80 ℃ until ready for use, when it was then plated on a sterilized Luria-Bertani (LB) agar plate and incubated overnight at 30 ℃. From the plate, 2 colonies were inoculated in 10 mL of LB broth overnight to reach the late log phase (OD_{600} =0.6-1.0). The bacteria were washed by centrifuging (10 min, 750×*g*), resuspended in D-PBS, and incubated at room temperature on a nutating mixer for 10 min. The bacteria were centrifuged again (10 min, 750×*g*), and resuspended in a HEPES buffer (2 mM HEPES, 25 mM NaCl, pH 7.4) to the appropriate OD_{600}.

2.6 Nanoparticle Dissolution in Bacterial Media

To measure how much iron dissolves in the HEPES buffer after one hour, suspensions in HEPES were made by mixing 450 µL of nanoparticle stock with 5.55 mL of HEPES buffer to a final concentration of 300 µg/mL of iron oxide. These were left at room temperature for one hour before being centrifuged at 4700×*g* for 30 min, followed by centrifuging the supernatant twice at 286,000×*g* for two hours. Removal of nanoparticles was confirmed with DLS, and the iron content of the supernatants was measured with the Thermo Scientific XSERIES 2 ICP-MS.

2.7 Drop plate Colony Counting Assays for Viability

To assess the viability of *S. oneidensis* MR-1 after exposure to the NPs, the bacterial OD_{600} in HEPES buffer was adjusted to 0.2 (which corresponds to ~2×10^8 bacterial cells/mL) and then diluted 1000-fold. To a suspension of bacteria (925 µL), NP treatments were added (75 µL), and exposures lasted for 1 h. Both iron-containing nanoparticles were used at iron concentrations of 300 µg/mL (as a control nanoparticle, the MSNs were used so that the silica mass matched that of the silica in msIONPs (4.7 mg/mL)). Six 10 µL drops of each suspension were dropped onto dried, UV-resterilized LB agar plates and incubated for ~17 h at 30 ℃. In separate experiments assessing the viability of bacteria after exposure to iron ions, iron (III) chloride hexahydrate was used for exposure concentrations of 7.6 and 1.0 ppb, to recreate the iron ion concentration determined to be released from IONPs and msIONPs, respectively. The number of colonies that

grew in each treatment were counted and recorded. These colony counts were normalized by dividing by the number of colonies that grow in the negative control samples to facilitate comparison between trials.

2.8 Nanoparticle Association with TEM

To visualize the binding of nanoparticles to *S. oneidensis*, the bacterial OD_{600} was adjusted to 0.8 (which corresponds to ~8×10^8 bacterial cells/mL) before mixing the bacterial suspension (925 µL) with nanoparticles (75 µL). The nanoparticles were used at the same concentrations as for colony counting experiments. After a one-hour exposure, the samples were centrifuged at 800×*g* for 5 min and the supernatant discarded.

The bacterial samples were prepared for TEM by adapting previously reported methods.[30,31] The samples were washed thrice without resuspension using 0.1 M cacodylate buffer, centrifuging at 500×*g* for 2 min between each wash step. To fix the sample, the pellet was resuspended in 2.5% glutaraldehyde in 0.1 M cacodylate buffer for 50 min, followed by centrifuging at 800×*g* for 5 min. The pellet was again washed three times with 0.1 M cacodylate buffer without resuspension. To dehydrate the samples, a series of ethanol washes was done at increasing ethanol concentrations in water, using each concentration twice (30%, 50%, 70%, 80%, 95%, and 100% ethanol). The samples were then washed three times with propylene oxide prior to using a 2:1 propylene oxide:resin mix for two hours, uncovered. This 2:1 mixture was replaced with 1:1 propylene oxide:resin to soak overnight, after which it was replaced with fresh 1:1 propylene oxide:resin for four hours. The samples were then incubated in pure resin overnight, which was replaced with fresh resin the next day. To cure the resin, the samples were put in a 40 ℃ oven for 24 h and a 60 ℃ oven for 48 h. The samples were sliced into ~70 nm thick sections using a LEICA EM UC6 ultramicrotome, which were stained with uranyl acetate and lead citrate. The slices were placed on 200 mesh copper grids with carbon and Formvar supports (Ted Pella, Inc., Redding, CA). Images of the samples were acquired using a FEI T12 transmission electron microscope at an operating voltage of 120 kV.

2.9 Nanoparticle Association using ICP-MS

To measure the amount of iron oxide nanoparticles and mesoporous silica-coated iron oxide nanoparticles that bind to *S. oneidensis*, the OD_{600} of bacteria was adjusted to be 0.2 (~2×10^8 bacterial cells/mL) and then exposed to nanoparticles by mixing 925 µL of bacterial suspension with 75 µL of nanoparticles to achieve final concentrations of 300 µg/mL of iron oxide. Control experiments were set up simultaneously that mixed HEPES buffer with nanoparticles. After the one-hour exposure, the samples were centrifuged twice at 800×*g*, discarding all but 50 µL of the supernatant since the pellet is easily disturbed. After the first centrifugation, the pellet was resuspended carefully in 1 mL HEPES buffer, and after the second centrifugation, the pellet was resuspended in 150 µL of HEPES buffer. The resuspended pellet (125 µL) was diluted with 375 µL of concentrated nitric acid (*Caution: use care when handling corrosive acids*) and the sample was digested at 60 ℃ overnight. The samples were t hen diluted 14-fold and centrifuged at 17,000×*g* for 20 min to remove bacterial cell debris. The samples were analyzed using the Thermo Scientific XSERIES 2 ICP-MS. To determine the amount of iron associated with the bacteria, the iron concentration detected in the respective control and the iron contribution by the bacteria were subtracted from the iron concentration in the experimental/bacterial samples, and then the dilutions were taken into account.

2.10 Riboflavin Secretion Measurements

A previous method was adapted to determine the amount of riboflavin secreted by bacteria after nanoparticle exposure.[32] To begin, the OD_{600} in HEPES buffer was adjusted to 0.2. The bacteria were then exposed to NPs for 1 h and then centrifuged at 17,000×*g* for 20 min to pellet both the bacteria and NPs. The supernatant was collected, and 200 µL was transferred to an HPLC vial with 250 µL glass insert. The supernatant was analyzed using an Agilent 1200 HPLC fitted with a Zorbax Eclipse XDB-C_{18} analytical column (4.6 x 150 mm, 5 µm packing material) and an Eclipse XDB-C_{18} analytical guard column (4.6 x 12.5 mm, 5 µm packing material) ahead of the fluorescence detector. Isocratic HPLC was performed with a mobile phase composed of 70/30

20 mM citric acid buffer (pH 3.3)/methanol with an injection volume of 30 µL, flow rate of 1 mL/min, and run time of 8 min. Excitation and emissions wavelengths of 450 and 530 nm, respectively, were used to detect riboflavin.

2.11 Extracting RNA from *S. oneidensis* after Nanoparticle Exposure

The RNA extraction was performed using a Zymo Research Direct-zol™ RNA MiniPrep Plus kit. To do the one-hour nanoparticle exposure prior to RNA extraction, the bacterial OD_{600} in HEPES buffer was adjusted to 1.0 (corresponding to ~1×10^9 bacterial cells/mL), and 1.85 mL of bacterial suspension was mixed with 150 µL of nanoparticle suspension (or water as a negative control), using nanoparticle concentrations that matched the colony counting experiments. Afterward, the suspensions were centrifuged at 2000×*g* for 10 min and the pellet was resuspended in 200 µL of RNAzol RT. Centrifugation at 16,000×*g* for 1 min removed particulate debris, and 200 µL of 200 proof molecular biology grade ethanol was added to the supernatant and mixed. This mixture was added to a Zymo-Spin IIC column in a collection tube and centrifuged at 16,000×*g* for 30 sec, discarding the flow through. To the column, 400 µL of RNA wash buffer was added and centrifuged at 16,000×*g* for 30 sec. To do a DNase I treatment, 5 µL of DNase I and 75 µL of DNA digestion buffer were mixed separately and then transferred to the column surface, incubating at room temperature for 15 min to digest DNA. Then, the column was washed twice by sequential additions of 400 µL of Direct-zol RNA PreWash and centrifuging at 16,000×*g* for 30 sec, discarding the flow through. 700 µL of RNA wash buffer was added to the column and centrifuged at 16,000×*g* for 2 min. The column was transferred to a clean, RNase-free Eppendorf tube where 80 µL of DNase/RNase-free water was added and centrifuged at 16,000×*g* for 30 sec to collect the RNA product. The concentration and quality of the RNA was measured using a Thermo Scientific NanoDrop™ One^C.

2.12 Monitoring Gene Expression Changes in *S. oneidensis* after Nanoparticle Exposure

Total purified RNA was reverse transcribed into complementary deoxyribonucleic acid (cDNA) as previously described.[33] cDNA was synthesized using 100 ng of total RNA template

and was incubated with an aliquot of deoxyribonucleotides and random primers at 65 ℃ for 5 min followed by chilling on ice for 1 min. SuperScript III reverse transcriptase, dithiothreitol, and RNaseOUT™ recombinant ribonuclease inhibitors were added into the mixture after the incubation following the temperature program of 25 ℃ for 5 min, 50 ℃ for 60 min, and 70 ℃ for 15 min for primer extension. Synthesized cDNA was then stored at -20 ℃.

Quantitative reverse transcription PCR was run to determine the expression levels of several genes involved in iron acquisition, storage, and utilization for *S. oneidensis*, with *radA* and *gyrB* genes serving as housekeeping genes for analysis. The list of genes used in this study can be found in the Supplementary Information (Table S1); these genes were selected to assess different aspects of the interaction between *S. oneidensis* and iron. An iQ5 real-time PCR detection system (Bio-Rad Laboratories) using SYBR Green for the fluorescent intercalating dye (iTaq™ Universal SYBR® Green Supermix) was used for this process. Each of the qPCR reactions containing cDNA (1 μL) mixed with primers (1 μL) with fluorescent dye (10 μL) and nuclease-free water (8 μL) was carried out in 96-well PCR plates, centrifuging the plates at 1000×*g* for 10 min at 4 ℃ prior to running the qPCR. The polymerase chain reactions started at 95 ℃ for 10 min for DNA denaturing, then underwent 40 real-time PCR amplification cycles (15 s at 95 ℃, followed by 30 s at 60 ℃). Fluorescenc e of the SYBR Green was then detected at the end of each PCR cycle. All samples were analyzed with technical duplicates.

3. Results and Discussion

3.1 Characterization of MSNs, IONPs, and msIONPs

The nanomaterials used in this study were characterized by a variety of methods. Using TEM, the morphology and size distribution of the materials could be determined (Figure 1). The mesoporous silica nanoparticles were found to have a diameter of 60 ± 15 nm (n=632), similar to the diameter of 57 ± 10 nm (n=521) found for mesoporous silica-coated iron oxide

nanoparticles. The purchased iron oxide nanoparticles were smaller, with a diameter of 12 ± 5 nm (n=557).

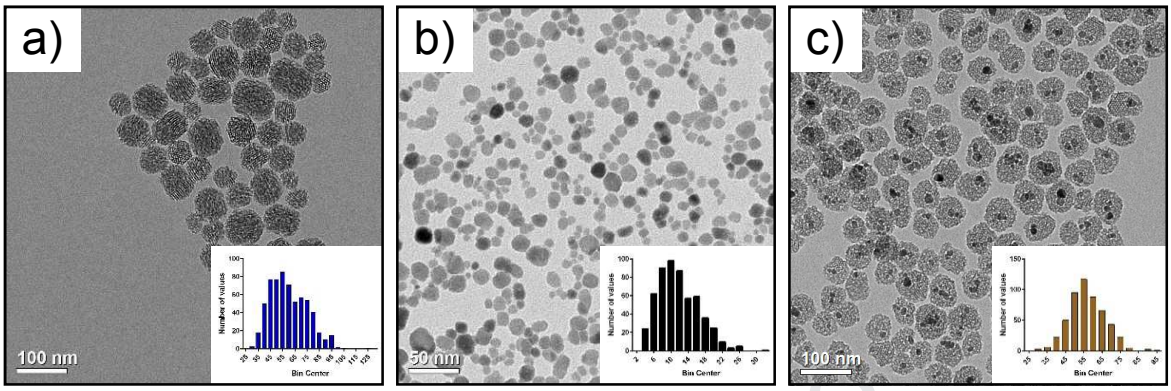

Figure 1. Transmission electron microscope images reveal the size and dispersity of a) mesoporous silica nanoparticles, b) iron oxide nanoparticles, and c) mesoporous silica-coated iron oxide nanoparticles. An inset in each image shows the size histogram determined for each nanoparticle type. Note that the scale bar for image (b) is half the size of that for the other two images.

The hydrodynamic diameters of the material were also determined for MSNs (86 ± 21 nm), msIONPs (90 ± 6 nm), and IONPs (55 ± 6 nm), reflecting the trend seen by TEM size analysis. The ζ-potential for msIONPs (-39 ± 12 mV) was more negative than that for MSNs (-18 ± 9 mV) or IONPs (-23 ± 15 mV); these values suggest that all three nanoparticle formulations should be relatively colloidally stable. In fact, throughout the course of the exposure experiment, all three nanoparticles were stable, as indicated by their unchanging hydrodynamic diameter in HEPES buffer over 2 h (Figure S1).

3.2 Impact of Nanoparticles on *S. oneidensis*

After a one-hour exposure to the different nanoparticles, the impact to *S. oneidensis* was assessed using a colony counting assay (Figure 2). The results demonstrate that while mesoporous silica-coated iron oxide nanoparticles and mesoporous silica nanoparticles have no impact on bacterial survival compared to the control, the iron oxide nanoparticles enhance the growth of the bacteria in HEPES buffer and therefore have an enhanced survival rate. Iron is an essential nutrient for bacteria,[34] thus it is reasonable that the presence of exogenous iron could enhance their growth. Specifically for *S. oneidensis* MR-1, iron oxide is a metal that they are

capable of respiring anaerobically as a means of obtaining energy;[9] alternately, dissolution product iron ions may contribute to bacterial sustenance. To probe the mechanism by which iron helps sustain bacteria in HEPES buffer, the contributions of the various means by which *S. oneidensis* can respire iron oxide were determined, as well as any impact of iron dissolution from the iron oxide nanoparticles. To evaluate how the mesoporous silica coating mitigates the impact by IONPs, effects on these endpoints by IONPs and msIONPs were compared.

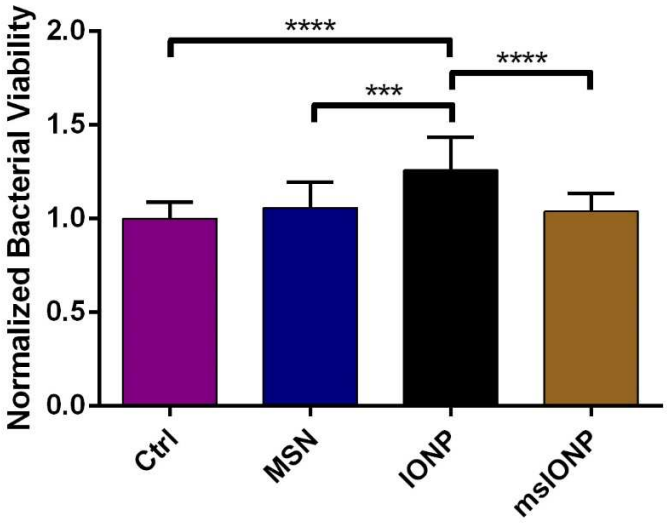

Figure 2. The colony counts determined from each nanoparticle type after being normalized to the control indicates that mesoporous silica and mesoporous silica-coated iron oxide nanoparticles have no impact on survival while the iron oxide nanoparticles enhance bacterial survival compared to a negative control. The error bars represent standard deviations from sixteen replicates. Statistical significance was evaluated using a one-way ANOVA with Tukey's multiple comparisons post-hoc test. ***p<0.001, ****p<0.0001

3.3 Differential Ion Release is Observed for Nanoparticles

To determine the concentrations of iron that were released from IONPs and msIONPs during their one-hour exposure to bacteria in HEPES buffer, ICP-MS was used to measure iron concentrations from an abiotic supernatant after removing the NPs from suspension. Results showed that IONPs released significantly more iron (7.6 ± 0.2 ppb) compared to msIONPs (1.0 ± 0.4 ppb) after an hour in HEPES buffer ($p<0.0001$). This observation suggests that a silica coating mitigates dissolution of the nanoparticle core.[35] While these results indicate the iron concentrations released from the nanoparticles, they do not specify the oxidation states of the

335 dissolved iron. MINTEQ modeling was used to show that at equilibrium, Fe^{3+} is the dominant
336 oxidation state for the dissolved iron (Table S2), prompting the use of iron (III) chloride
337 hexahydrate for the ion control studies performed.

338 **3.4 Iron Ion Exposure Recapitulates Effect Seen by Nanoparticles**

339 *S. oneidensis* were exposed to the concentrations of iron ions released during nanoparticle
340 exposure, and their viability was assessed using the colony counting assay. From this assay, it
341 was seen that the iron ion exposure recapitulates the results of nanoparticle exposure, with the
342 iron ion concentrations equivalent to the release from the control and msIONP trials both
343 showing a similar viability around 1.0, and the iron ion concentrations equivalent to release from
344 IONPs showing an increased bacterial survival (Figure 3). The bacterial viability after exposure
345 to the ion concentration representing IONP exposure was 1.24±0.27, which is not statistically
346 distinct from the 1.26±0.18 viability seen after exposure to IONPs. These comparisons
347 demonstrate that the dissolved ion constituents of these nanoparticles are dominating the
348 observed effect of the nanoparticles on *S. oneidensis*. In addition, these results show that, since
349 the presence of a mesoporous silica coating reduces dissolution to levels that do not impact *S.*
350 *oneidensis*, this reduced dissolution is the major contributor to the mechanism by which the
351 mesoporous silica coating mitigates IONP impact.

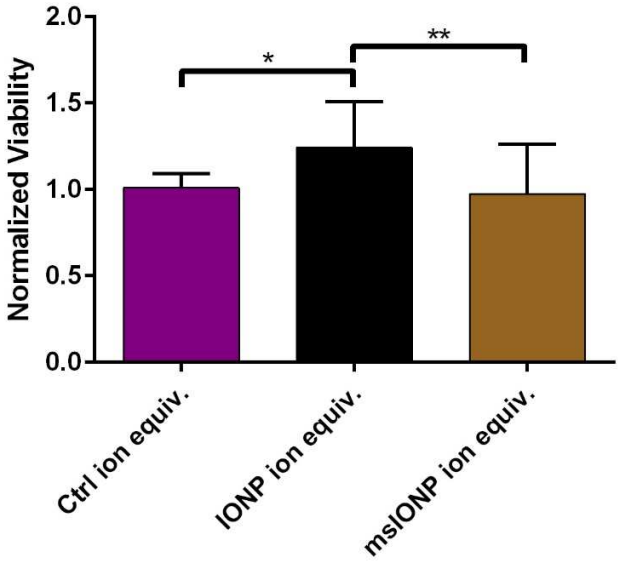

Figure 3. At Fe^{3+} ion concentrations that match those released during nanoparticle exposure, it can be seen that 7.6 ppb iron ions (equivalent to the released concentration from IONPs) are enhancing bacterial survival to the same extent as observed with IONP exposure, while at 1.0 ppb (equivalent to the released concentration from msIONPs), no impact on growth is observed. These data demonstrate that the impact from the iron ions is recapitulating the impact observed from the nanoparticle exposures, and therefore ion dissolution is the main contributor to the nanoparticles' effects. The error bars represent the standard deviations from fifteen replicate trials. One-way ANOVA with Tukey's multiple comparisons test was used to evaluate statistical significance. *p<0.05, **p<0.01

3.5 IONPs Display Significant Binding to the Bacterial Surface

While the ion studies indicate that ion release is the major contributor to the impacts of the nanoparticles, the other mechanisms by which *S. oneidensis* can interact with iron oxide nanoparticles were assessed as well. Some of these mechanisms involve direct binding with the cell wall, thus, the interactions of the NPs with bacteria were visualized by first fixing the samples and embedding them in resin. Images of the resin-embedded samples were then acquired with TEM. For samples containing IONPs and msIONPs, the TEM was performed in dark-field mode to verify that nanoparticles were observed by taking advantage of the scattering efficiency of crystalline iron oxide nanoparticles.[36] These images clearly show that the IONPs are binding to *S. oneidensis* to a greater extent than MSNs or msIONPs (Figure 4). Given that all three nanoparticles used in this study have a negative surface charge, which often leads to electrostatic repulsion from the net-negative charge of the bacterial membrane, it is not

surprising that there is no interaction between the membrane and MSNs or msIONPs. However, it is interesting that there is such prevalent binding of IONPs, which implies specific interactions by the bacteria with this material.

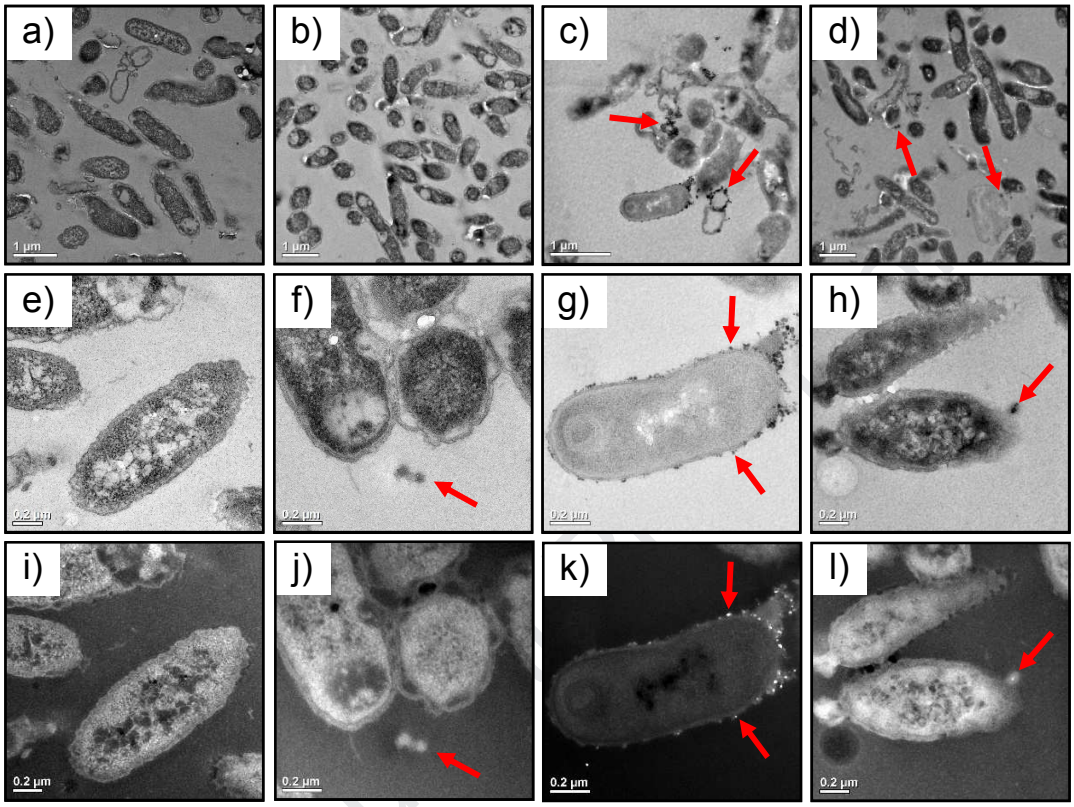

Figure 4. A low magnification view of bacteria after exposure to a) nanoparticle-free suspension, b) MSNs, c) IONPs, and d) msIONPs as well as a high magnification view of e) NP-free suspension, as well as bacteria exposed to f) MSNs, g) IONPs, and h) msIONPs reveal that there is more binding with IONPs than the other two nanomaterials. No instance of direct binding by MSNs could be found, which indicates that if they do occur, they are a rare occurrence. Where present, instances of nanoparticles in each image are highlighted with arrows. Dark-field images of i) NP-free bacteria are included as a comparison to bacteria exposed to j) MSNs, k) IONPs, and l) msIONPs. The bright points are due to the high scattering efficiency of IONPs in both images and are not seen in the control image. Mesoporous silica nanoparticles do not exhibit the same scattering intensity in dark-field mode due to their noncrystalline nature.

Beyond the visual evidence from TEM, quantitative evidence of increased IONP binding was acquired by exposing the bacteria to nanoparticles, pelleting the bacteria, and digesting them to quantify the amount of iron material that was associated with the bacteria (likely the surface, based on TEM data). Since iron quantitation was the endpoint, this does not reveal anything about the binding of MSNs to the bacterial surface. Corroborating the TEM images, a significant increase in iron content from bacteria that were exposed to IONPs was found compared to

those that were exposed to msIONPs (Figure 5). In fact, msIONPs displayed bacterial association that was not statistically different from the negative control. These quantitative data demonstrate that *S. oneidensis* is bound to 0.9% of the available NPs when exposed to IONPs and to 0.01% of the available msIONPs in that exposure. This was calculated by dividing the bound iron mass by the total iron content present in each exposure.

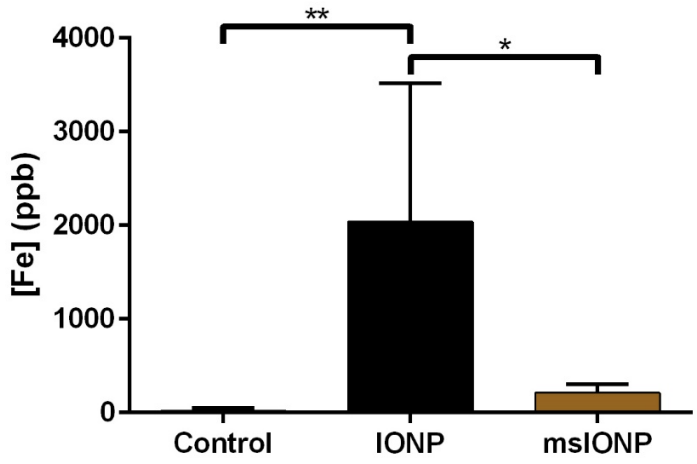

Figure 5. The iron content determined from bacteria that had been exposed to IONPs and msIONPs shows that there is significant iron bound to the surface of IONP-exposed bacteria. Statistical testing was performed with a one-way ANOVA of at least three replicates, using Tukey's multiple comparisons test to compare the effects of each treatment. *p<0.05, **p<0.01

Taken together, these data show that there is significantly more binding of IONPs to the bacterial surface than MSNs or msIONPs. While this observation is important, it was shown in Section 3.4 that the bacterial viability after exposure to nanoparticles was recapitulated by the released iron ions, demonstrating that this increased association has negligible contributions to the effects of IONPs to bacterial survival. Therefore, while coating the IONPs with a mesoporous silica shell does reduce the association, this reduced physical association does not contribute to the mitigation of the impact of IONPs on bacterial viability.

3.6 Riboflavin Production is Unchanged by Nanoparticle Exposure

Riboflavin secretion is one method by which *S. oneidensis* is capable of respiring extracellular iron oxide. To assess the mechanism that extracellular electron shuttling via

riboflavin secretion is contributing to the beneficial impacts seen with IONP exposure, the production of riboflavin in bacteria was monitored via HPLC. Secreted riboflavin, which elutes around 6.3 min with the separation method used, was measured from all of the samples; however, it is noted that the secretion of riboflavin from *S. oneidensis* is not changed by the presence of any of the nanomaterials (Figure 6). Given that riboflavin is secreted by bacteria to perform extracellular electron transfers to respire metals, these findings indicate that this riboflavin-mediated extracellular electron transport mechanism is not a major contributor to the beneficial impact seen with IONPs.

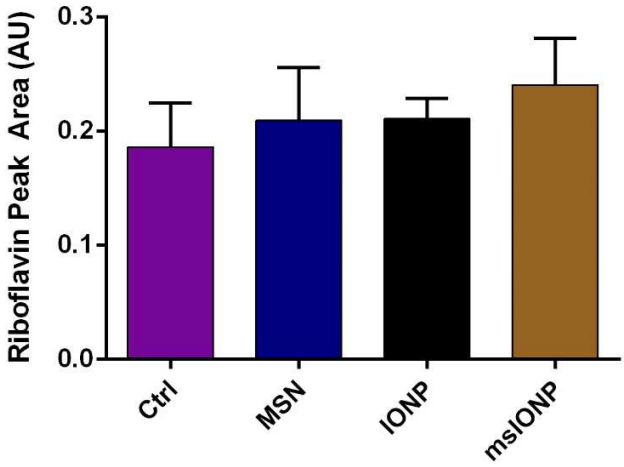

Figure 6. The secretion of riboflavin by *S. oneidensis* is not impacted by exposure to any of the nanomaterials used in this study. The error bars represent the standard deviations from six replicates. One-way ANOVA with Tukey's multiple comparisons test was used to determine statistical significance between the treatments.

3.7 Changes in Gene Expression are Nanoparticle-Specific

Since it is clear that *S. oneidensis* is using the iron oxide nanoparticles, it was expected that there would be changes in gene expression of bacterial genes relating to the transport, storage, and utilization of iron after exposure to IONPs and their released ion equivalents. To probe this, changes in gene expression after exposure to nanoparticles or to the released iron ion equivalents were monitored using RT-qPCR (Figure 7). There was no noted change in the expression of *ribBA*, whose function is in the synthesis of riboflavin. This corroborates the lack

of increased production of riboflavin after NP exposure in the HPLC analysis shown in Figure 6, and verifies that this mechanism is not contributing significantly to the impact of IONPs on *S. oneidensis*. Most of the genes that encode for proteins that are associated with the membrane of the bacteria, *exbB*, *tonB*, *feoA,* have been upregulated by IONPs and msIONPs. However, *pubA,* which does not encode for a membrane-associated protein, was also upregulated after nanoparticle treatment. Instead, *pubA,* encodes for a siderophore that complexes with ferric iron and shuttles it back to the bacterial cell for storage via a TonB-dependent siderophore receptor, which suggests that its function is still related to processes at the bacterial surface.[37] Given that *exbB* and *tonB* both have functions related to the intracellular uptake of iron,[38] it is clear that *S. oneidensis* is working to sequester at least some of the extra iron that it is encountering in the presence of the IONPs or msIONPs; however, the increased bacterial association seen with IONPs helps to facilitate this process better than with msIONPs. For the gene, *ftn*, which corresponds with iron sequestration, there is no change in expression noted, which makes sense given that in an iron-rich environment, the bacterium would not need to store it for later use. Conversely, for *bfd*, a gene that encodes for a protein that initiates use of sequestered iron, upregulation is observed. An interesting observation is that there is increased expression of *feoA*, which is specific for ferrous ion transport into the bacterial cell.[39] Since our MINTEQ calculations showed that the oxidation state of the majority of released iron would be Fe^{3+}, the increased *feoA* expression suggests that *S. oneidensis* may be processing the nanoparticles to make ferrous ion, which is then transported into the bacterial cell for use. The fact that gene expression changes after exposure to IONPs and msIONPs appear to be very similar, and yet only IONP exposure is aiding bacterial survival, indicates that while genes for iron uptake and usage are being upregulated in both exposures, there is more iron present in the IONP exposures for the bacteria to actually use. This highlights the fact that gene expression changes are more sensitive to environmental changes than more macro-level endpoints such as overall bacterial survival.

These observed gene expression changes appear to be nanoparticle-specific, as treatment with equivalent doses of released ions did not induce the same changes. In fact, exposure to ions caused very few gene expression changes, with just a few genes being downregulated upon exposure to 1 ppb Fe^{3+}. We speculate that the observed association of the nanoparticles to the bacteria may be initiating these gene expression changes by dissolving to form a higher localized concentration of iron ions right at the bacterial surface, especially if the bacteria are also assisting in the dissolution by processing the nanoparticles to generate ferrous ion, as suggested by the upregulation of *feoA*.

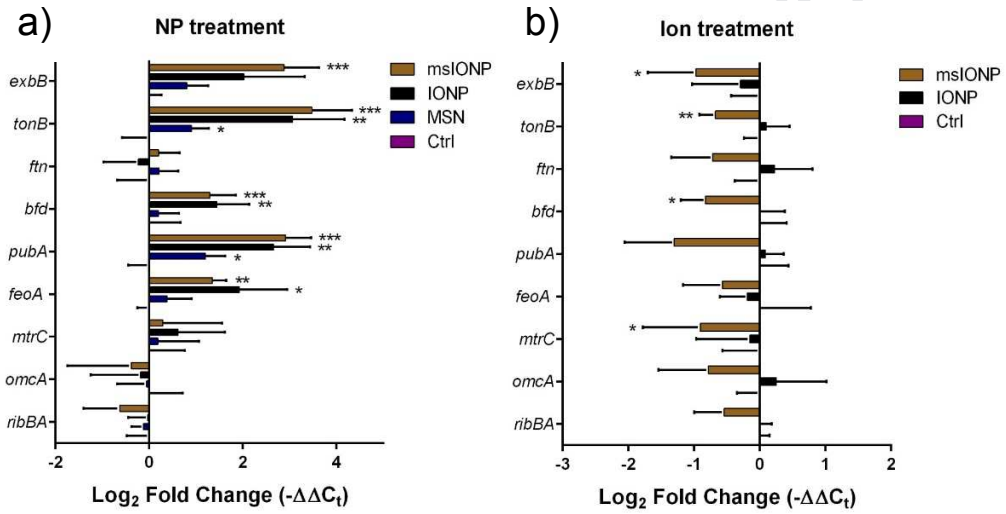

Figure 7. Gene expression changes in *S. oneidensis* after exposure to a) nanoparticles and b) equivalent released ion concentrations. The error bars represent standard deviations from five replicates. One-way ANOVA with a Dunnett's multiple comparisons test was used to determine statistical significance between the different treatments and the control. *p<0.05, **p<0.01, ***p<0.001

4. Conclusions

The work presented herein investigates the impact of IONPs and their mesoporous silica-coated counterparts on *S. oneidensis.* After exposure to the nanoparticles, colony counting reveals that IONPs promote bacterial survival. Exposing *S. oneidensis* to ferric ion at a dose equivalent to released iron from IONPs and msIONPs recapitulates the viability seen with nanoparticle exposure, indicating that ion release is the major contributor to the bacterial impact of IONPs. As expected, the presence of a mesoporous silica shell on IONPs reduced the iron dissolution

observed, which explains the mitigated impact on viability of msIONPs on the bacteria. Association between the nanoparticles and *S. oneidensis* shows that there is the greatest bacterial association with IONPs, with minimal association with msIONPs or MSNs. Interestingly, while the ions account for the enhanced bacterial survival after exposure to the nanoparticles, at the genetic level, a nanoparticle-specific effect is observed since the ion controls did not induce the same gene expression changes. Given that the genes impacted upon nanoparticle exposure mostly encode for membrane-associated proteins, we speculate that the observed association of nanoparticles with the bacterial membrane may cause upregulation of these genes. This could be due to a higher localized concentration of iron released near the bacterial surface or simply due to the direct interaction between the nanoparticles and bacterial membrane. Since perturbations to the environment, whether by increasing or decreasing survival for select organisms, can be detrimental in some situations, the mesoporous silica-coated iron oxide nanoparticles are deemed here to be a better option for sustainability. Given that a mesoporous silica shell should reduce dissolution for other core materials, this strategy could also be applied to more toxic NPs whose major toxicity mechanism is related to dissolution of ions, where it would similarly be expected to reduce harmful impacts to organisms.

5. Acknowledgements

This work was supported by the National Science Foundation under the Center for Sustainable Nanotechnology, CHE-1503408. The CSN is part of the Centers for Chemical Innovation Program. J.T.B. acknowledges support by a National Science Foundation Graduate Research Fellowship (grant number 00039202). TEM imaging in this study was carried out in the Characterization Facility, University of Minnesota, which receives partial support from the National Science Foundation through the MRSEC program. The authors are grateful to Fang Zhou at the Characterization Facility for microtome preparation of resin-embedded samples for TEM. The authors gratefully acknowledge Elizabeth Lundstrom for ICP-MS analysis of the NP

binding samples as well as the iron dissolution samples as part of the University of Minnesota Earth Sciences Department. The authors thank Dr. Erin Carlson for use of her iQ5 real-time PCR detection system.

6. Competing Interests

The authors declare no competing financial interest.

Corresponding author

*Prof. Christy Haynes, University of Minnesota, chaynes@umn.edu, (612) 626-1096

ORCID IDs of Authors

Joseph T. Buchman: 0000-0001-5827-8513

Thomas Pho: 0000-0001-6131-2233

Rebeca S. Rodriguez: 0000-0002-8994-554X

Z. Vivian Feng: 0000-0002-3329-3781

Christy L. Haynes: 0000-0002-5420-5867

7. Supplementary Information

Materials used; list of genes analysed in gene expression studies; stability of nanoparticles in exposure medium; MINTEQ evaluation of dissolved iron species; representative HPLC chromatograms.

8. References

(1) Teja, A. S.; Koh, P. Y. Synthesis, Properties, and Applications of Magnetic Iron Oxide Nanoparticles. *Prog. Cryst. Growth Charact. Mater.* **2009**, *55*, 22–45.

(2) Alcantara, D.; Lopez, S.; García-Martin, M. L.; Pozo, D. Iron Oxide Nanoparticles as Magnetic Relaxation Switching (MRSw) Sensors: Current Applications in Nanomedicine. *Nanomedicine Nanotechnology, Biol. Med.* **2016**, *12*, 1253–1262.

(3) Liu, H.; Zhang, J.; Chen, X.; Du, X.-S.; Zhang, J.-L.; Liu, G.; Zhang, W.-G. Application of Iron Oxide Nanoparticles in Glioma Imaging and Therapy: From Bench to Bedside.

Nanoscale **2016**, *8*, 7808–7826.

(4) Hurley, K. R.; Lin, Y.-S.; Zhang, J.; Egger, S. M.; Haynes, C. L. Effects of Mesoporous Silica Coating and Postsynthetic Treatment on the Transverse Relaxivity of Iron Oxide Nanoparticles. *Chem. Mater.* **2013**, *25*, 1968–1978.

(5) Jeon, S.; Oberreit, D. R.; Van Schooneveld, G.; Gao, Z.; Bischof, J. C.; Haynes, C. L.; Hogan, C. J. Ion-Mobility-Based Quantification of Surface-Coating-Dependent Binding of Serum Albumin to Superparamagnetic Iron Oxide Nanoparticles. *ACS Appl. Mater. Interfaces* **2016**, *8*, 24482–24490.

(6) Gao, Z.; Burrows, N. D.; Valley, N. A.; Schatz, G. C.; Murphy, C. J.; Haynes, C. L. In Solution SERS Sensing Using Mesoporous Silica-Coated Gold Nanorods. *Analyst* **2016**, *141*, 5088–5095.

(7) Hurley, K. R.; Ring, H. L.; Etheridge, M.; Zhang, J.; Gao, Z.; Shao, Q.; Klein, N. D.; Szlag, V. M.; Chung, C.; Reineke, T. M.; Garwood, M.; Bischof, J. C.; Haynes, C. L. Predictable Heating and Positive MRI Contrast from a Mesoporous Silica-Coated Iron Oxide Nanoparticle. *Mol. Pharm.* **2016**, *13*, 2172–2183.

(8) Hau, H. H.; Gralnick, J. A. Ecology and Biotechnology of the Genus *Shewanella*. *Annu. Rev. Microbiol.* **2007**, *61*, 237–258.

(9) Xiong, Y.; Shi, L.; Chen, B.; Mayer, M. U.; Lower, B. H.; Londer, Y.; Bose, S.; Hochella, M. F.; Fredrickson, J. K.; Squier, T. C. High-Affinity Binding and Direct Electron Transfer to Solid Metals by the *Shewanella oneidensis* MR-1 Outer Membrane *c*-Type Cytochrome OmcA. *J. Am. Chem. Soc.* **2006**, *128*, 13978–13979.

(10) Myers, J. M.; Myers, C. R. Role for Outer Membrane Cytochromes OmcA and OmcB of *Shewanella putrefaciens* MR-1 in Reduction of Manganese Dioxide. *Appl. Environ. Microbiol.* **2001**, *67*, 260–269.

(11) Shi, L.; Richardson, D. J.; Wang, Z.; Kerisit, S. N.; Rosso, K. M.; Zachara, J. M.; Fredrickson, J. K. The Roles of Outer Membrane Cytochromes of *Shewanella* and

Geobacter in Extracellular Electron Transfer. *Environ. Microbiol. Rep.* **2009**, *1*, 220–227.

(12) Marsili, E.; Baron, D. B.; Shikhare, I. D.; Coursolle, D.; Gralnick, J. A.; Bond, D. R. *Shewanella* Secretes Flavins That Mediate Extracellular Electron Transfer. *Proc. Natl. Acad. Sci.* **2008**, *105*, 3968–3973.

(13) Fredrickson, J. K.; Romine, M. F.; Beliaev, A. S.; Auchtung, J. M.; Driscoll, M. E.; Gardner, T. S.; Nealson, K. H.; Osterman, A. L.; Pinchuk, G.; Reed, J. L.; Rodionov, D. A.; Rodrigues, J. L. M.; Saffarini, D. A.; Serres, M. H.; Spormann, A. M.; Zhulin, I. B.; Tiedje, J. M. Towards Environmental Systems Biology of *Shewanella*. *Nat. Rev. Microbiol.* **2008**, *6*, 592–603.

(14) Gorby, Y. A.; Yanina, S.; McLean, J. S.; Rosso, K. M.; Moyles, D.; Dohnalkova, A.; Beveridge, T. J.; Chang, I. S.; Kim, B. H.; Kim, K. S.; Culley, D. E.; Reed, S. B.; Romine, M. F.; Saffarini, D. A.; Hill, E. A.; Shi, L.; Elias, D. A.; Kennedy, D. W.; Pinchuk, G.; Watanabe, K.; Ishii, S.; Logan, B.; Nealson, K. H.; Fredrickson, J. K. Electrically Conductive Bacterial Nanowires Produced by *Shewanella oneidensis* Strain MR-1 and Other Microorganisms. *Proc. Natl. Acad. Sci.* **2006**, *103*, 11358–11363.

(15) Bretschger, O.; Obraztsova, A.; Sturm, C. A.; Chang, I. S.; Gorby, Y. A.; Reed, S. B.; Culley, D. E.; Reardon, C. L.; Barua, S.; Romine, M. F.; Zhou, J.; Beliaev, A. S.; Bouhenni, R.; Saffarini, D.; Mansfeld, F.; Kim, B.-H.; Fredrickson, J. K.; Nealson, K. H. Current Production and Metal Oxide Reduction by *Shewanella oneidensis* MR-1 Wild Type and Mutants. *Appl. Environ. Microbiol.* **2007**, *73*, 7003–7012.

(16) Fukushima, T.; Gupta, S.; Rad, B.; Cornejo, J. A.; Petzold, C. J.; Chan, L. J. G.; Mizrahi, R. A.; Ralston, C. Y.; Ajo-Franklin, C. M. The Molecular Basis for Binding of an Electron Transfer Protein to a Metal Oxide Surface. *J. Am. Chem. Soc.* **2017**, *139*, 12647–12654.

(17) Perez-Gonzalez, T.; Jimenez-Lopez, C.; Neal, A. L.; Rull-Perez, F.; Rodriguez-Navarro, A.; Fernandez-Vivas, A.; Iañez-Pareja, E. Magnetite Biomineralization Induced by *Shewanella oneidensis*. *Geochim. Cosmochim. Acta* **2010**, *74*, 967–979.

(18) Perez-Gonzalez, T.; Valverde-Tercedor, C.; Yebra-Rodriguez, A.; Prozorov, T.; Gonzalez-Muñoz, M. T.; Arias-Peñalver, J. M.; Jimenez-Lopez, C. Chemical Purity of *Shewanella oneidensis*-Induced Magnetites. *Geomicrobiol. J.* **2013**, *30*, 731–748.

(19) Coker, V. S.; Pearce, C. I.; Pattrick, R. A. D.; Van Der Laan, G.; Telling, N. D.; Charnock, J. M.; Arenholz, E.; LLoyd, J. R. Probing the Site Occupancies of Co-, Ni-, and Mn-Substituted Biogenic Magnetite Using XAS and XMCD. *Am. Mineral.* **2008**, *93*, 1119–1132.

(20) Luo, H.-W.; Zhang, X.; Chen, J.-J.; Yu, H.-Q.; Sheng, G.-P. Probing the Biotransformation of Hematite Nanoparticles and Magnetite Formation Mediated by *Shewanella oneidensis* MR-1 at the Molecular Scale. *Environ. Sci. Nano* **2017**, *4*, 2395–2404.

(21) Liu, J.; Pearce, C. I.; Shi, L.; Wang, Z.; Shi, Z.; Arenholz, E.; Rosso, K. M. Particle Size Effect and the Mechanism of Hematite Reduction by the Outer Membrane Cytochrome OmcA of *Shewanella oneidensis* MR-1. *Geochim. Cosmochim. Acta* **2016**, *193*, 160–175.

(22) Kostka, J. E.; Nealson, K. H. Dissolution and Reduction of Magnetite by Bacteria. *Environ. Sci. Technol.* **1995**, *29*, 2535–2540.

(23) Venkateswaran, K.; Moser, D. P.; Dollhopf, M. E.; Lies, D. P.; Saffarini, D. A.; MacGregor, B. J.; Ringelberg, D. B.; White, D. C.; Nishijima, M.; Sano, H.; Burghardt, J.; Stackebrandt, E.; Nealson, K. H. Polyphasic Taxonomy of the Genus *Shewanella* and Description of *Shewanella oneidensis* sp. nov. *Int. J. Syst. Bacteriol.* **1999**, *49*, 705–724.

(24) Roberts, J. A.; Fowle, D. A.; Hughes, B. T.; Kulczycki, E. Attachment Behavior of *Shewanella putrefaciens* onto Magnetite under Aerobic and Anaerobic Conditions. *Geomicrobiol. J.* **2006**, *23*, 631–640.

(25) Kasai, T.; Kouzuma, A.; Nojiri, H.; Watanabe, K. Transcriptional Mechanisms for Differential Expression of Outer Membrane Cytochrome Genes *omcA* and *mtrC* in *Shewanella oneidensis* MR-1. *BMC Microbiol.* **2015**, *15*, 68.

(26) Zhang, H.; Fu, H.; Wang, J.; Sun, L.; Jiang, Y.; Zhang, L.; Gao, H. Impacts of Nitrate and

Nitrite on Physiology of *Shewanella oneidensis*. *PLoS One* **2013**, *8*, e62629.

(27) Yuan, J.; Chen, Y.; Zhou, G.; Chen, H.; Gao, H. Investigation of Roles of Divalent Cations in *Shewanella oneidensis* Pellicle Formation Reveals Unique Impacts of Insoluble Iron. *Biochim. Biophys. Acta* **2013**, *1830*, 5248–5257.

(28) Lin, Y.-S.; Abadeer, N.; Hurley, K. R.; Haynes, C. L. Ultrastable, Redispersible, Small, and Highly Organomodified Mesoporous Silica Nanotherapeutics. *J. Am. Chem. Soc.* **2011**, *133*, 20444–20457.

(29) Schneider, C. A.; Rasband, W. S.; Eliceiri, K. W. NIH Image to ImageJ: 25 Years of Image Analysis. *Nat. Methods* **2012**, *9*, 671–675.

(30) Schrand, A. M.; Schlager, J. J.; Dai, L.; Hussain, S. M. Preparation of Cells for Assessing Ultrastructural Localization of Nanoparticles with Transmission Electron Microscopy. *Nat. Protoc.* **2010**, *5*, 744–757.

(31) Buchman, J. T.; Rahnamoun, A.; Landy, K. M.; Vartanian, A. M.; Jacob, L. M.; Murphy, C. J.; Hernandez, R.; Haynes, C. L. Using an Environmentally-Relevant Panel of Gram-Negative Bacteria to Assess the Toxicity of Polyallylamine Hydrochloride-Wrapped Gold Nanoparticles. *Environ. Sci. Nano* **2018**, *5*, 279–288.

(32) Maurer-Jones, M. A.; Gunsolus, I. L.; Meyer, B. M.; Christenson, C. J.; Haynes, C. L. Impact of TiO_2 Nanoparticles on Growth, Biofilm Formation, and Flavin Secretion in *Shewanella oneidensis*. *Anal. Chem.* **2013**, *85*, 5810–5818.

(33) Qiu, T. A.; Bozich, J. S.; Lohse, S. E.; Vartanian, A. M.; Jacob, L. M.; Meyer, B. M.; Gunsolus, I. L.; Niemuth, N. J.; Murphy, C. J.; Haynes, C. L.; Klaper, R. D. Gene Expression as an Indicator of the Molecular Response and Toxicity in the Bacterium *Shewanella oneidensis* and the Water Flea *Daphnia magna* Exposed to Functionalized Gold Nanoparticles. *Environ. Sci. Nano* **2015**, *2*, 615–629.

(34) Andrews, S. C. Iron Storage in Bacteria. In *Advances in Microbial Physiology*; 1998; Vol. 40, pp 281–351.

(35) Mahoney, S.; Najera, M.; Bai, Q.; Burton, E. A.; Veser, G. The Developmental Toxicity of Complex Silica-Embedded Nickel Nanoparticles Is Determined by Their Physicochemical Properties. *PLoS One* **2016**, *11*, e0152010.

(36) Klein, N. D.; Hurley, K. R.; Feng, Z. V.; Haynes, C. L. Dark Field Transmission Electron Microscopy as a Tool for Identifying Inorganic Nanoparticles in Biological Matrices. *Anal. Chem.* **2015**, *87*, 4356–4362.

(37) Liu, L.; Li, S.; Wang, S.; Dong, Z.; Gao, H. Complex Iron Uptake by the Putrebactin-Mediated and Feo Systems in *Shewanella oneidensis*. *Appl. Environ. Microbiol.* **2018**, *84*, e01752-18.

(38) Noinaj, N.; Guillier, M.; Barnard, T. J.; Buchanan, S. K. TonB-Dependent Transporters: Regulation, Structure, and Function. *Annu. Rev. Biochem.* **2010**, *64*, 43–60.

(39) Lau, C. K. Y.; Krewulak, K. D.; Vogel, H. J. Bacterial Ferrous Iron Transport: The Feo System. *FEMS Microbiol. Rev.* **2016**, *40*, 273–298.

9. TOC Graphic

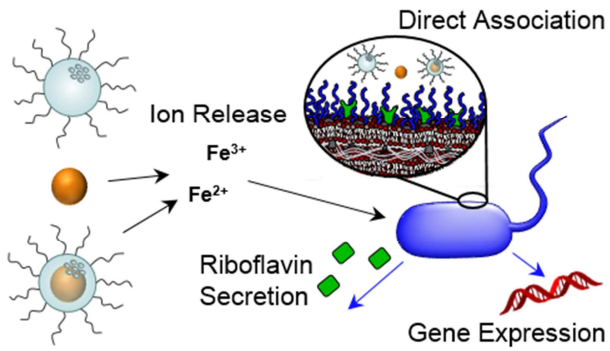

Highlights

- Iron oxide nanoparticles enhance survival of the bacterium, *Shewanella oneidensis*.
- Dissolved iron released from IONPs recapitulates growth pattern observed with NP exposure.
- A mesoporous silica coating reduces IONP dissolution, thus mitigating their impact.
- Changes in gene expression demonstrate a nanoparticle-specific effect.